DOI: 10.1002/ejic.200700708

Complexation of 2,6-Bis(3-pyrazolyl)pyridine–Bis(thiocyanato)iron(II) with a Bridging 4,4′-Bipyridine: A New Example of a Dinuclear Spin Crossover Complex

Dalila Fedaoui,[a,b] Yacine Bouhadja,[b] Abdellah Kaiba,[b] Philippe Guionneau,[b] Jean-François Létard,*[b] and Patrick Rosa*[b]

Keywords: Spin crossover / Magnetic properties / Iron / Dinuclear complexes

Investigation of the coordination behavior of 2,6-bis(3-pyrazolyl)pyridine–bis(thiocyanato)iron(II) towards bridging ligands led to the discovery of a novel dinuclear complex showing spin-crossover. Chemical and structural characterization and a first report of physical properties are presented.

Introduction

Research efforts into the spin-crossover phenomenon have reached new heights recently, as industrial applications (memories, optical devices, etc.) seem to be quite near at-hand.[1] Obviously, the possibility goes through a deeper understanding of the physics involved, and various research groups have focused on increasing this understanding, more specifically on relaxation processes of metastable states and cooperativity effects.[2] Chemists are feeding this effort through the design and synthesis of novel molecules, and on-going efforts are directed towards the synthesis of oligonuclear complexes,[3] which can show behavior not accessible to mononuclear or 1D, 2D, and 3D structures.[4] One of the obvious difficulties of such a project is the very sensitivity of the spin-crossover phenomenon to slight changes in the formulation,[5] the geometry, the crystal packing, and the synthetic procedure.[6]

Within our research group, we have been trying to adopt a "molecular-bricks" approach to this problem by starting from known ligands showing promising behavior and by considering them either as blocking or bridging ligands. In this frame, the bis(pyrazolyl)pyridine (bpp) family is a very interesting candidate. Bpp ligands, close to the widely used terpirydine, have shown many instances of homoleptic complexes of Fe^{II} with spin-crossover behavior[7] and interesting photomagnetic behavior.[5b,8] Most importantly for us, they are frameworks amenable to more sophisticated functionalization.[7,9] One roadblock that remains though is whether heteroleptic complexes of Fe^{II} with spin-crossover properties can be synthesized to gain access to more sophisticated structures. We decided to explore the coordination of those ligands with Fe^{II} complexed with anionic monodentate coligands such as thiocyanate, which can block two positions of octahedral Fe^{II}. It thus prevents the formation of homoleptic complexes, but it also leaves one free position for a monodentate ancillary ligand, which allows the Fe^{II} ligand field to be tuned. This paper reports the successful synthesis through this design strategy of the bis[2,6-bis(3-pyrazolyl)-pyridine]–4,4′-bipyridinetetrathiocyanatodiiron(II) methanol adduct, which is a novel spin-transition dinuclear complex in which 4,4′-bipyridine acts as bridging ligand, with full chemical characterization. Preliminary structural and photomagnetic properties of this compound are also reported.

Results and Discussion

Synthesis and Crystal Structure

The complex was synthesized following the procedure reported in Scheme 1. Preformed bis(thiocyanato)iron(II) reacts in methanol with the 3-bpp [3-bpp = 2,6-bis(3-pyrazolyl)pyridine] ligand at room temperature. The ensuing red solution was then cannulated into a dichloromethane solution of 4,4′-bipyridine. Stirring at room temperature shows the formation of a red precipitate, which was isolated by filtration in good yield. Microanalysis showed that the expected formulation as only a dinuclear complex was not satisfactory, as in fact the complex precipitates as a solvent (methanol) adduct. The insertion of solvent into the lattice was probably to be expected because the 3-bpp ligand has

[a] Department of Chemistry, University of Annaba, Sidi-Ammar 23200, Algeria
[b] ICMCB, CNRS, Université Bordeaux 1
87, avenue du Dr. A. Schweitzer 33608 Pessac cedex, France
Fax: +33-540002649
E-mail: rosa@icmcb-bordeaux.cnrs.fr

Supporting information for this article is available on the WWW under http://www.eurjic.org or from the author.

two pendant amine protons that usually bond to protic donors.[8a–8c] The infrared spectrum of the powder showed only one absorption in the cyanide region at 2079 cm^{-1}, which supports a *trans* coordination of the thiocyanate on each iron center. We then sought to obtain X-ray diffraction quality crystals in order to gain more insight into the structure and the crystal packing of the complex.

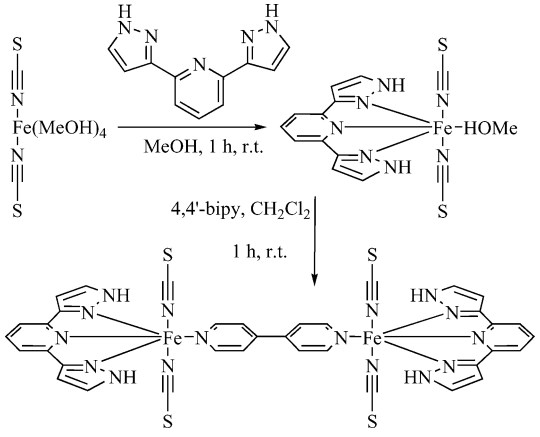

Scheme 1.

Suitable crystals of high quality were straightforwardly obtained by diffusion techniques. The resulting resolved X-ray structure is presented in Figure 1. The complex crystallizes in the centrosymmetric $P2_1/n$ space group, with an inversion center lying in the middle of the 4.4′-bipyridine moiety. Thus, Figure 1 actually shows two asymmetric units with the previously supposed dinuclear structure and *trans* coordination of the thiocyanate units. The methanol molecules are hydrogen-bonded to one of the free amine nitrogen atoms of each 3-bpp ligands. The pyridine of the bridging 4,4′-bipyridine is thus forced to twist (relatively to the plane of the opposing 3-bpp) to meet the steric requirements of the methanol, and the iron atom is thrown off the plane of this pyridine by 0.297 Å.[10] Furthermore, the N_{py}–Fe–N_{py} angle [171.732(55)°] shows that this pyridine bends away from the methanol molecule towards the free amine. This accounts for the fact that there is only one molecule of methanol per 3-bpp ligand in the complex.

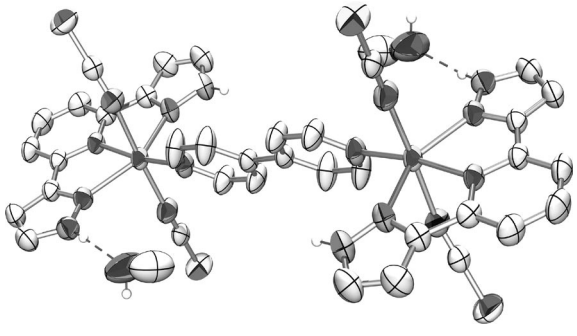

Figure 1. ORTEP diagram of bis[2,6-bis(3-pyrazolyl)pyridine]–4,4′-bipyridinetetrathiocyanatodiiron(II) methanol adduct; thermal ellipsoids are cut at the 50% probability level. Hydrogen atoms were omitted for clarity. Hydrogen bonds between the amine nitrogen atoms and methanol are represented as dashed lines. For relevant bonds lengths and angles see text.

The Fe–N bond lengths are typical of a high-spin Fe^{II}:[11] Fe–NCS 2.108(2) and 2.1548(19) Å, Fe–bipy 2.1689(16) Å, and Fe–bpp 2.1482(15) Å for the pyridine and 2.2084(18) and 2.233(2) Å for the pyrazoles. Thus, the metal surroundings can be described as a distorted octahedron tetragonally elongated along the weakest pyrazole ligands; the iron atom is only 0.056 Å off the mean plane of the nitrogen atoms of the pyridine moieties and the NCS ligands, and the N–Fe–N angles are close to 90° at 95.73(6), 83.65(6), 91.94(7), and 88.52(7)°.

The crystal packing is represented in Figure 2. Careful examination reveals a dense network of intermolecular contacts. A complete description of those contacts is given in the Supporting Information (Table S1 and Figures S2–S6). Generally, the Fe–Fe axis lies close to the *c* axis and the thiocyanate moieties lie close to the *a* axis; the intramolecular Fe–Fe distance is 11.4133(19) Å.

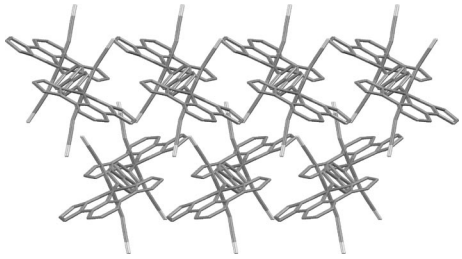

Figure 2. Representation of the crystal packing viewed along the *c* axis. Hydrogen atoms and methanol were omitted for clarity.

The complexes are thus organized in sheets parallel to the *bc* plane. Within these sheets, links in both the *b* and *c* directions occur through π interactions[12] and C–H···π contacts[13] between hydrogen atoms of one pyrazole and an adjacent thiocyanate. When considering one half of the complex (the asymmetric unit), one pyrazole is stacked with an adjacent pyrazole along the *b* axis [shortest distance 3.370(4) Å][14] and stacked with the central pyridine of another bpp ligand along the *c* axis [shortest distance 3.438(4) Å];[15] the hydrogen atom in the 4-position is close to the adjacent thiocyanate along the *b* axis [C···C 3.796(3) Å]. Symmetrically, the bpp pyridine is stacked along the *c* axis and the other pyrazole along the *b* axis. Another C–H···π interaction along the *b* axis occurs between the pyrazole hydrogen in the 5-position and the adjacent thiocyanate [C···C 3.495(3) Å].

The sheets are connected through strong interactions, mainly hydrogen bonds, along the *a* axis and along the [1–11] axis (see Table S1 and Figure S2–S4). Along the *a* direction, the available amine hydrogens of the pyrazole ring enter into hydrogen bonding with the thiocyanate ligands, either directly [N···$^-$S 3.425(2) Å] or mediated by a molecule of methanol [N···O 2.786(3) Å, O···S^- 3.405(4) Å].

Variable-Temperature Measurements: Diffuse Reflectivity and Magnetic Susceptibility

The behavior of the complex with variable temperature was studied with a homemade diffuse reflectivity setup. Results on a powder sample are presented in Figure 3. Two main features are visible in the diffuse-absorption spectra. On the high-energy end, a strong absorption takes place below 600 nm, which corresponds to both the MLCT (metal-to-ligand charge transfer) and the d–d bands of the LS (low-spin) state of the complex. The other absorption band centered around 820 nm is very likely to be the d–d transition band of the HS (high-spin) state.[16]

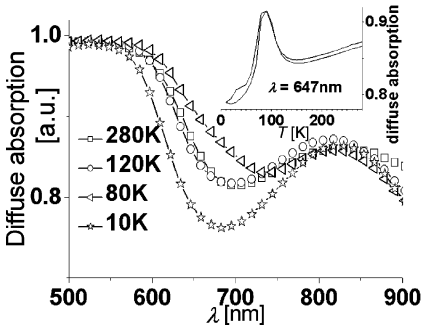

Figure 3. Variable-temperature diffuse absorption spectra in the range 450–950 nm; inset: diffuse absorbance signal vs. T measured at 647 nm.

A decrease in the temperature down to 120 K only led to sharpening of this low-energy band. A further decrease in the temperature to 80 K led to some changes in the valley around 700 nm and an apparent shift in the high-energy band towards lower energy, which can also be interpreted as the apparition of a new band, as was previously seen.[3e] At 10 K, the band at 800 nm again shifted towards higher energy. This can be illustrated graphically, as our instrumental set-up allows the reflectance/absorbance to be monitored at a given wavelength. The inset in Figure 3 shows the result of such a measurement at 647 nm. Significant changes occurred between 120 and 80 K and then again below 80 K. Those changes can be generally associated to spin crossover occurring at the surface of the solid for the former, and to some form of photoconversion, that is to the LIESST effect, for the latter.[1d,8f]

We then proceeded to confront those results with magnetic susceptibility measurements. Results are shown in Figure 4. As seen in the variable-temperature reflectance, no significant change occurred between room temperature and 120 K. At 250 K, the value measured for the product χT of 7.4 $cm^3 K mol^{-1}$ is in agreement with two fully high-spin S = 2 centers in a HS–HS state and a Landé factor g = 2.22; this value is typical for highly anisotropic Fe^{II} atoms. Between 120 and 70 K, χT decreases to 4.7 $cm^3 K mol^{-1}$, which is a value that is close to half of that seen at higher temperatures. Similar plots were observed in other dinuclear systems.[3d,3h] This variation can only be accounted for either by one of the two iron atoms in each complex undergoing spin crossover or by having one half of the complexes undergoing complete spin crossover. As to which hypothesis is correct remains to be ascertained, as well as whether crossover of fully half the iron atoms or less than half occur. Below 60 K, the χT value decreases again to 3.6 $cm^3 K mol^{-1}$ at 10 K. This further decrease is most certainly due to the high zero-field splitting of the remaining Fe^{II} center[17] and is very unlikely at those temperatures to be caused by further spin crossover of the remaining high-spin centers. Likewise, some antiferromagnetic exchange can be dismissed, as the shortest iron–iron distance is intermolecular at 7.960(1) Å along the c direction and the contact is only mediated through π stacking.[15]

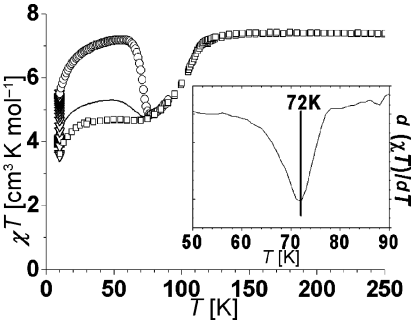

Figure 4. Product of magnetic susceptibility χ with temperature between 10 and 200 K [open squares, in the dark; open triangles, under irradiation at 10 K; solid line, for T(LIESST) measurement after irradiation at 830 nm; and open circles, for T(LIESST) measurement after irradiation at 647 nm]; inset: T(LIESST) for the measurement at 647 nm.

The findings of the variable-temperature diffuse reflectivity measurement were checked by irradiating the sample in situ at 10 K either with a 830-nm laser diode or with the 647-nm band of a Kr^+ laser. For either wavelength, an increase in the magnetic moment was seen, which shows the presence of the LIESST effect for this compound; irradiation was faster and more efficient at 647 nm than it was at 830 nm (after 180 min at this wavelength the magnetic moment does not saturate). This latter behavior could be due to competition between population of the metastable high-spin state by LIESST and depopulation by reverse-LIESST,[16] where at this wavelength both the borderline of the LS state MLCT band and the HS state d–d band are superimposed. Thus, upon irradiation at 647 nm for 70 min, χT saturates at 5.5 $cm^3 K mol^{-1}$. By proceeding to measure the T(LIESST) temperature,[1d,8f] we noticed that χT increased slowly up to a plateau at 7.2 $cm^3 K mol^{-1}$ between 50–60 K; this value is comparable to the one measured at room temperature, which would point towards almost complete photoconversion. It then fell back down to the values observed for the thermal transition. The inflexion point gave a T(LIESST) value of 72 K.

The thermal spin transition is not particularly abrupt; thus, it gave no evidence for a strong cooperative behavior in the solid. Also, the shape of the T(LIESST) curve reflecting the relaxation of the metastable photoinduced state is relatively gradual. The absence of cooperativity for the photoinduced HS state is further evidenced by the diffuse

reflectivity measured at 647 nm (Figure 3, inset). We further checked the existence of a light-induced thermal hysteresis (LITH, see Figure S7), which depends on some degree of cooperative behavior.[18] Only a small hysteresis with a width of 6 K[19] can be measured while irradiating at 647nm.

This complex is thus a new example of a spin-crossover dinuclear complex. It can be compared to the dinuclear complexes synthesized by Real and coworkers that were also shown to undergo the LIESST effect.[4] Irradiation was also shown in this case to induce full photoconversion to a metastable HS–HS state, and the magnetic susceptibility curve was interpreted as showing an antiferromagnetic interaction mediated by the bipyrimidine bridge. The analysis of that interaction is quite difficult due to the orbitally degenerate $^5T_2$ ground state of octahedral Fe^{II}. If one neglects the resulting anisotropy, interactions of –4 to –6 cm^{-1} are found for a Fe–Fe distance close to 6 Å.[20] If anisotropy is taken into account as single-ion anisotropy, then the interaction is greatly reduced, for example, at –1.1(1) cm^{-1} for d(Fe–Fe) = 5.918(2) Å.[21] In our case, with an intramolecular Fe–Fe distance of more than 10 Å and with the shortest intermolecular distances being more than 7 Å, it is clear that whatever interaction there is should be too small to be accurately determined by fits on magnetic susceptibility measurements.[22]

Conclusions

We synthesized a new example of a quite restricted ensemble: a dinuclear Fe^{II} compound showing spin crossover and the LIESST effect. The crossover is only partial, and Mössbauer measurements are underway to quantify the proportion of high-spin and low-spin Fe atoms in both low-temperature and high-temperature phases. The availability of crystals led us to undertake a full variable-temperature crystallographic study of this compound, which will be reported in due course. The kinetics and the cooperative behavior of the photoinduced state still remain to be studied.

Experimental Section

General: C, H, N, and S microanalysis was performed with a ThermoFischer Flash EA1112. Fe microanalysis was performed with a Varian ES-720 ICP-OES. IR spectra were measured as KBr pellet with a Perkin–Elmer PARAGON1000 FTIR spectrometer. Synthesis was performed by using standard Schlenk techniques under an atmosphere of nitrogen. Freshly distilled solvents were used; methanol was distilled from Mg and CH_2Cl_2 from CaH_2.

Representative Synthetic Procedure: A solution of $Fe(H_2O)_7(SO_4)$ (232mg, 0.83mmol), KSCN (162 mg, 1.67 mmol), and a few grains of ascorbic acid (to reduce trace amounts of Fe^{3+} in Fe^{2+}) in MeOH (10 mL) was stirred for 1 h and then filtered through a frit under an atmosphere of nitrogen. This solution was then cannulated into a solution of 3-bpp (176 mg, 0.83 mmol) in MeOH (4 mL). The resulting solution became red immediately. After 1 h, a solution of 4,4′-bipyridine (65 mg, 0.42 mmol) in dichloromethane (2 mL) was added through a cannula. A red precipitate formed after 15 min. This suspension was stirred for 45 min before it was filtered through a frit under an atmosphere of nitrogen. The resulting red powder was left to dry on the bench. Yield: 308 mg (75%). IR (KBr): $\tilde{\nu}$ = 2076, 2079 cm^{-1}. [{Fe(3-bpp)$(NCS)_2$}$_2$(4,4′-bipy)]·2MeOH: $C_{38}H_{34}Fe_2N_{16}O_2S_4$ (986.74): calcd. C 46.25, H 3.47, Fe 11.32, N 22.71, S 13.00; found C 45.72, H 3.46, Fe 11.94, N 22.95, S 12.91. Deep-red, well-formed, single-crystal prisms can be easily obtained in a few days by layering a freshly prepared solution of Fe(3-bpp)$(NCS)_2$(MeOH) in methanol over a solution of 4,4′-bipyridine in dichloromethane in a Schlenk tube under an atmosphere of nitrogen.

X-ray Analysis: A single crystal with approximate dimensions of $0.37 \times 0.30 \times 0.15$ mm^3 was mounted on a Bruker-Nonius κ-CCD diffractometer, Mo-K_α radiation (0.71073 Å). Data collection was performed at 293 K by using mixed ϕ and ω scans, 440 s per frame and a distance crystal-detector of 26 mm. The structural determination by direct methods and the refinement of atomic parameters based on full-matrix least-squares on F_2 were performed by using the SHELX-97[23] programs within the WINGX package.[24] Results: monoclinic $P2_1/n$ space group, a = 15.683(2) Å, b = 8.160(1) Å, c = 18.597(3) Å, β = 110.140(5)°, V = 2234.4(6) $Å^3$, $D_{calcd.}$ = 1.467, 99.3% completeness to θ 26.37°, 14702 collected data, 3923 independent observed reflections with $I > 2\sigma(I)$ (R_{int} = 0.0220) for 327 refined parameters, R_{all} = 0.0416, R_{obs} = 0.0348, wR_{2obs} = 0.0908, $(\Delta/\sigma)_{max}$ = 0.001, S = 1.059, residual electronic densities ρ_{max} = 0.327 and ρ_{min} = –0.449 e $Å^{-3}$. Methanol solvent molecules show some disorder that could not be fit satisfactorily with a two-site model. Hydrogen bonded to nitrogen atoms could be located, and the remaining ones were calculated. CCDC-653178 contains the supplementary crystallographic data for this paper. These data can be obtained free of charge from The Cambridge Crystallographic Data Centre via www.ccdc.cam.ac.uk/datarequest/cif.

Physical Measurements: Diffuse absorption spectra and reflectivity signal measurements were performed with a homemade set-up equipped with a SM240 spectrometer (Opton Laser International). This set-up allows both the diffuse absorption spectra within the range of 500–900 nm at a given temperature and the temperature dependence (5–290 K) of the reflectivity signal at a selected wavelength (±2.5 nm) to be recorded. Diffuse reflectance spectra were calibrated against activated charcoal (Merck) as a black standard and barium sulfate ($BaSO_4$, Din 5033, Merck) as a white standard. Analyses were performed on thin layers of available solid samples as polycrystalline powders; no dispersion in a matrix was required. Photomagnetic experiments were carried out with a Quantum Design MPMS-5S magnetometer working in the dc mode. The measurements were performed in the 5–300 K range with a magnetic field of 20 kOe for χT. Photomagnetic experiments were performed with either a Kr^+ laser or a laser diode coupled through an optical fiber into the SQUID cavity. A small amount of powder was laid down on a sample holder. The diamagnetic contribution and the weight were estimated by comparing the $\chi T(T)$ curve with one recorded for the powdered sample in a routine experiment (15 mg of sample). These comparisons give m = 285 μg and diamagnetic correction = $-8{,}49.10^{-3}$ emu mol^{-1}. The sample was irradiated continuously by using either the 647 nm line of the Kr^+ laser or the 830 nm laser diode, under a magnetic field of 20 kOe at 10 K, until magnetization saturation was obtained. The output power laser light was 60 mW cm^{-2}, which corresponds to the effective power received by the measured sample to ≈3 mW cm^{-2}. The

procedures for LIESST and LITH measurement were described elsewhere.[1d,8f,18c]

Supporting Information (see footnote on the first page of this article): Tables of van der Waals contacts and hydrogen bonds and representations of those contacts; LITH measurement under 647-nm laser irradiation.

Acknowledgments

The authors wish to thank CNRS, Région Aquitaine, and EU NEX MAGMANET for funding. L. Etienne from ICMCB is gratefully acknowledged for ICP-OES measurements.

[1] a) O. Kahn, J. Martinez, *Science* **1998**, *279*, 44–48; b) O. Sato, S. Hayami, Y. Einaga, Z. Z. Gu, *Bull. Chem. Soc. Jpn.* **2003**, *76*, 443–470; c) J. F. Létard, P. Guionneau, L. Goux-Capes in *Topics in Current Chemistry Vol. 235: Spin Crossover in Transition Metal Compounds III* (Eds.: P. Gütlich, H. A. Goodwin), Springer, Berlin, **2004**, pp. 221–249; d) J.-F. Létard, P. Guionneau, O. Nguyen, J. Sanchez Costa, S. Marcen, G. Chastanet, M. Marchivie, L. Goux-Capes, *Chem. Eur. J.* **2005**, *11*, 4582–4589; e) E. Freysz, S. Montant, S. Létard, J. F. Létard, *Chem. Phys. Lett.* **2004**, *394*, 318–323; f) S. Cobo, G. Molnar, J. A. Real, A. Bousseksou, *Angew. Chem. Int. Ed.* **2006**, *45*, 5786–5789.

[2] a) A. Hauser, *J. Chem. Phys.* **1991**, *94*, 2741–2748; b) A. Hauser, A. Vef, P. Adler, *J. Chem. Phys.* **1991**, *95*, 8710–8717; c) A. Hauser, J. Jeftic, H. Romstedt, R. Hinek, H. Spiering, *Coord. Chem. Rev.* **1999**, *190–192*, 471–491; d) J. F. Létard, J. Sanchez Costa, S. Marcen, C. Carbonera, C. Desplanches, A. Kobayashi, N. Daro, P. Guionneau, J. P. Ader, *J. Phys: Conf. Ser.* **2005**, *21*, 23–29; e) N. O. Moussa, G. Molnar, S. Bonhommeau, A. Zwick, S. Mouri, K. Tanaka, J. A. Real, A. Bousseksou, *Phys. Rev. Lett.* **2005**, *94*, 107205/1–107205/4; f) R. Boca, W. Linert, *Monatsh. Chem.* **2003**, *134*, 199–216; g) K. Boukheddaden, M. Nishino, S. Miyashita, F. Varret, *Phys. Rev. B Condens. Matter* **2005**, *72*, 014467/1–014467/11; h) K. Xiao-Yu, Z. Kang-Wei, *J. Phys. Chem. A* **2005**, *109*, 10129–10137.

[3] Dinuclear complexes: a) K. S. Murray, C. J. Kepert in *Topics in Current Chemistry Vol. 233: Spin Crossover in Transition Metal Compounds I* (Eds.: P. Gütlich, H. A. Goodwin), Springer, Berlin, **2004**, pp. 195–228; b) B. Weber, E. Kaps, *Heteroat. Chem.* **2005**, *16*, 391–397; c) F. Tuna, M. R. Lees, G. J. Clarkson, M. J. Hannon, *Chem. Eur. J.* **2004**, *10*, 5737–5750; d) S. R. Batten, J. Bjernemose, P. Jensen, B. A. Leita, K. S. Murray, B. Moubaraki, J. P. Smith, H. Toftlund, *Dalton Trans.* **2004**, 3370–3375; e) G. Chastanet, C. Carbonera, C. Mingotaud, J.-F. Létard, *J. Mater. Chem.* **2004**, *14*, 3516; f) C. J. Schneider, J. D. Cashion, B. Moubaraki, S. M. Neville, S. R. Batten, D. R. Turner, K. S. Murray, *Polyhedron*, DOI: 10.1016/j.poly.2006.09.003; g) K. Nakano, N. Suemura, K. Yoneda, S. Kawata, S. Kaizaki, *Dalton Trans.* **2005**, 740–743; h) A. B. Gaspar, M. C. Munoz, J. A. Real, *J. Mater. Chem.* **2006**, *16*, 2522–2533.

[4] a) E. Trzop, M. Buron-Le Cointe, H. Cailleau, L. Toupet, G. Molnar, A. Bousseksou, A. B. Gaspar, J. A. Real, E. Collet, *J. Appl. Crystallogr.* **2007**, *40*, 158–164; b) G. Chastanet, J.-F. Létard, A. B. Gaspar, J. A. Real, *Chem. Commun.* **2001**, 819–820; c) V. Ksenofontov, H. Spiering, S. Reiman, Y. Garcia, A. B. Gaspar, N. Moliner, J. A. Real, P. Gutlich, *Chem. Phys. Lett.* **2001**, *348*, 381–386.

[5] For example, see: a) K. H. Sugiyarto, D. C. Craig, A. D. Rae, H. A. Goodwin, *Aust. J. Chem.* **1994**, *47*, 869–890; b) S. Marcen, L. Lecren, L. Capes, H. A. Goodwin, J. F. Létard, *Chem. Phys. Lett.* **2002**, *358*, 87–95.

[6] P. Gütlich, *Struct. Bonding (Berlin)* **1981**, *44*, 83–195.

[7] M. A. Halcrow, *Coord. Chem. Rev.* **2005**, *249*, 2880–2908.

[8] a) T. Buchen, P. Gütlich, H. A. Goodwin, *Inorg. Chem.* **1994**, *33*, 4573–4576; b) T. Buchen, P. Gütlich, K. H. Sugiyarto, H. A. Goodwin, *Chem. Eur. J.* **1996**, *2*, 1134–1138; c) V. A. Money, J. Sanchez Costa, S. Marcen, G. Chastanet, J. Elhaik, M. A. Halcrow, J. A. K. Howard, J. F. Létard, *Chem. Phys. Lett.* **2004**, *391*, 273–277; d) V. A. Money, J. Elhaik, M. A. Halcrow, J. A. K. Howard, *Dalton Trans.* **2004**, 1516–1518; e) C. Carbonera, J. Sanchez Costa, V. A. Money, J. Elhaik, J. A. K. Howard, M. A. Halcrow, J. F. Létard, *Dalton Trans.* **2006**, 3058–3066; f) J. F. Létard, C. Carbonera, E. Courcot, J. Sanchez Costa, *Bull. Mater. Sci.* **2006**, *29*, 567–571.

[9] J. Elhaik, C. M. Pask, C. A. Kilner, M. A. Halcrow, *Tetrahedron* **2007**, *63*, 291–298.

[10] For comparison, the iron is only 0.082 Å off the plane of the 3-bpp pyridine ring plane. For pyrazole, which is a weaker ligand, those distances go up to 0.143 and 0.243 Å.

[11] P. Guionneau, M. Marchivie, G. Bravic, J. F. Létard, D. Chasseau in *Topics in Current Chemistry Vol. 234: Spin Crossover in Transition Metal Compounds II* (Eds.: P. Gütlich, H. A. Goodwin), Springer, Berlin, **2004**, pp. 97–128.

[12] C. Janiak, *J. Chem. Soc., Dalton Trans.* **2000**, 3885–3896.

[13] J. F. Malone, C. M. Murray, M. H. Charlton, R. Docherty, A. J. Lavery, *J. Chem. Soc. Faraday Trans.* **1997**, *93*, 3429–3436, M. F. Perutz, Philos., *Trans. R. Soc. London Ser. A* **1993**, *345*, 105–112, T. Steiner, *Angew. Chem. Int. Ed.* **2002**, *41*, 48–76.

[14] Distance between pyrazole centroids 3.845(3) Å; angle between mean planes 10.15(10)°; displacement angle[12] 23.71(8)°. See Supporting Information.

[15] Distance between pyrazole and pyridine centroids 3.763(4) Å; angle between mean planes 2.23(8)°; displacement angle[12] 25.92(5)°. See Supporting Information.

[16] A. Hauser, *J. Chem. Phys.* **1991**, *94*, 2741–2748.

[17] E. I. Solomon, E. G. Pavel, K. E. Loeb, C. Campochiaro, *Coord. Chem. Rev.* **1995**, *144*, 369–460.

[18] a) J. F. Létard, P. Guionneau, L. Rabardel, J. A. K. Howard, A. E. Goeta, D. Chasseau, O. Kahn, *Inorg. Chem.* **1998**, *37*, 4432–4441; b) A. Desaix, O. Roubeau, J. Jeftic, J. G. Haasnoot, K. Boukheddaden, E. Codjovi, J. Linares, M. Nogues, F. Varret, *Eur. Phys. J. B* **1998**, *6*, 183–193; c) J. F. Létard, G. Chastanet, O. Nguyen, S. Marcen, M. Marchivie, P. Guionneau, D. Chasseau, P. Gütlich, *Monatsh. Chem.* **2003**, *134*, 165–182.

[19] Because the LITH curve is essentially a kinetic phenomenon, the width was taken as the gap between the inflexion points of the downwards and the upwards curves.

[20] See Table 8 in J. Sletten, H. Daraghmeh, F. Lloret, M. Julve, *Inorg. Chim. Acta* **1998**, *279*, 127–135.

[21] $D = -17(2)$ cm^{-1} and $g = 2.24$, see J. S. Sun, H. Zhao, X. Ouyang, R. Clérac, J. A. Smith, J. M. Clemente-Juan, C. Gómez-Garcia, E. Coronado, K. R. Dunbar, *Inorg. Chem.* **1999**, *38*, 5841–5855.

[22] No maximum characteristic of an antiferromagnetic interaction is seen in the $\chi(T)$ curve. Fits of $\chi(T)$ and $\chi T(T)$ with a fully isotropic model give values below 1 cm^{-1}.

[23] G. M. Sheldrick, *Programs for Crystal Structure Analysis* (Release 97–2), Institut für Anorganische Chemie der Universität, University of Göttingen, Germany, **1998**.

[24] L. J. Farrugia, *J. Appl. Crystallogr.* **1999**, *32*, 837.

Received: July 6, 2007
Published Online: January 15, 2008

